



# Coercivity analysis of magnetic phases in sapropel S1 related to variations in redox conditions, including an investigation of the $S$ ratio

**Pauline P. Kruiver**

Paleomagnetic Laboratory, Fort Hoofddijk, Budapestlaan 17, 3584CD Utrecht, Netherlands (kruiver@geo.uu.nl)

**Hilde F. Passier**

Paleomagnetic Laboratory, Fort Hoofddijk, Budapestlaan 17, 3584CD Utrecht, Netherlands

Now at IWACO, Water Resources and Ecology, Rotterdam, Netherlands

[1] **Abstract:** The most recent sapropel (S1) in the eastern Mediterranean has been extensively investigated with geochemical and rock-magnetic techniques. Different redox conditions prevailed in different zones of the sediment through time. The oxidized sapropel zone is particularly interesting, because earlier studies indicated that new magnetic material was formed, including possible magnetosomes. Here we utilize component analyses of isothermal remanent magnetization (IRM) acquisition curves and the analysis of first-order reversal curves (FORC) to further investigate the magnetic mineralogy. In the entire box core ABC26, the original input of eolian dust consisted of both magnetite and hematite. In the oxidized sapropel and in the active oxidation zone, an additional magnetite component is present. This magnetite component has a higher coercivity than the eolian magnetite and a very small coercivity dispersion, suggesting a narrow grain size distribution. This is a strong indication that magnetosomes, which are formed in the active oxidation zone, are the magnetic carriers of this coercivity fraction. FORC diagrams support these findings. The  $S$  ratio is forwardly modeled for mixed magnetic mineralogies with varying coercivity distributions to explain the down core  $S$  ratio behavior: close to 1 in the top sediment and in the oxidized sapropel, a drop in values in the active oxidation zone, and again close to 1 in the (syn)sapropel. The observed  $S$  ratio pattern in the oxidized sapropel and in the active oxidation zone can be explained by the recovered IRM components. Whereas both oxidized sapropel and active oxidation zone contain the extra magnetite component, their  $S$  ratios are different because of the differences in coercivity characteristics (coercivity and dispersion) of the two magnetites in these zones. Thus, in these zones the  $S$  ratio does not reflect variations in the relative contributions of hematite to magnetite but variations in the characteristics of the individual magnetite assemblages. Also in the rest of the core, the  $S$  ratio depends on the coercivity characteristics of the magnetite component rather than on the relative contributions of high- versus low-coercivity minerals. The  $S$  ratio thus appears to be an unsuitable parameter to describe variations in the magnetic mineralogy, especially when more than two components are present. Therefore the classical interpretation of the  $S$  ratio should be treated with caution.

**Keywords:** Rock magnetism; isothermal remanent magnetization; magnetosomes; sapropel; FORC analysis;  $S$  ratio.

**Index terms:** Biomagnetism; rock and mineral magnetism; marine sediments.

**Received** 15 May 2001; **Revised** 8 August 2001; **Accepted** 28 September 2001; **Published** 14 December 2001.

Kruiver, P. P., and H. F. Passier, 2001. Coercivity analysis of magnetic phases in sapropel S1 related to variations in redox conditions, including an investigation of the  $S$  ratio, *Geochem. Geophys. Geosyst.*, vol. 2, Paper number 2001GC000181, 14 December 2001.

## 1. Introduction

[2] Sapropels form interesting environments from geochemical, climatic, and rock-magnetic points of view. They have been formed in the eastern Mediterranean periodically since the Pliocene [Emeis *et al.*, 1996]. Their formation is linked to enhanced productivity and increased preservation of organic matter during precession-induced insolation maxima when climate is relatively wet [Rossignol-Strick *et al.*, 1982; Rohling, 1994]. They are enriched in both organic carbon and pyrite, the latter as a result of bacterial sulfate reduction that prevailed during their deposition. Sapropels were anoxic and sulfidic during deposition. Sapropel formation ends upon reoxygenation of the bottom waters. Subsequently, the sapropel becomes buried under oxic sediments. Directly after burial, oxidation affects the sapropel, starting at the top and progressing downward. This sequence of anoxic to oxic conditions seriously affects magnetic minerals, because iron oxides are sensitive to redox conditions. Iron oxides dissolve in suboxic and anoxic conditions, whereas they precipitate in active zones of oxidation. Several studies show that iron oxides in the vicinity of (paleo)redox fronts have high coercivities [Tarduno and Wilkison, 1996; Tarduno *et al.*, 1998; Passier *et al.*, 2001], which could indicate the presence of bacterial magnetites [Moskowitz, 1993]. Abundant bacterial magnetites related to redox boundaries have been reported in deep-sea sediments as well [Schwartz *et al.*, 1997; Haese *et al.*, 1998].

[3] The most recent sapropel (S1) has been investigated extensively with geochemical and

rock-magnetic techniques [Passier, 1998; Passier *et al.*, 2001]. One of the most important magnetic features is the presence of high-coercivity signals (median destructive fields,  $B_{cr}$ ,  $B_c$ ) in the oxidized part of the sapropel. Low-temperature measurements strongly suggest that this signal is caused by magnetosomes consisting of magnetite that have been formed during oxidation (H. F. Passier and M. J. Dekkers, Assessment of the formation of iron oxides in the active oxidation front above sapropel S1 in the eastern Mediterranean Sea by low-temperature magnetic properties, submitted to *Geophysical Journal International*, 2001) (hereinafter referred to as Passier and Dekkers, submitted manuscript, 2001). The  $S$  ratio [Bloemendal *et al.*, 1992] is also affected in the zone of active oxidation, where it drops significantly below 1. In the classical interpretation of the  $S$  ratio this would indicate an increase in high-coercive material relative to low-coercive minerals. However, in the oxidized sapropel the  $S$  ratio remains close to one, whereas the high-coercivity signal is present in this layer as well.

[4] The present study utilizes analyses of isothermal remanent magnetization (IRM) components [Kruiver *et al.*, 2001] to examine the remanent magnetic mineralogy in and around sapropel S1 in core ABC26. Also, we apply the recently developed first-order reversal curve (FORC) technique [Pike *et al.*, 1999; Roberts *et al.*, 2000] to investigate magnetic mineralogy and domain state. The FORC technique provides an extra indication that the newly formed magnetic material in the oxidized sapropel and in the active oxidation zone indeed consists of magnetosomes.

Moreover, the theoretical analysis of the  $S$  ratio combined with the  $S$  ratio data for this core suggests that the  $S$  ratio is not a suitable parameter to analyze magnetic mixtures of more than two magnetic components. We find that the  $S$  ratio depends on the coercivity characteristics (mean coercivity and dispersion) of the magnetite coercivity components rather than on the relative contributions of high- versus low-coercivity phases.

## 2. Diagenesis and Rock Magnetism of Sapropel S1

[5] Rock-magnetic evidence for diagenetic processes around sapropel formation and subsequent burial for the eastern Mediterranean box core ABC26 (Figure 1) is described by *Passier et al.* [2001] and Passier and Dekkers (submitted manuscript, 2001). A number of processes that have affected the magnetic material have played a role during formation and burial of the sediments. This resulted in five geochemically different zones (from top to bottom): (1) the top sediment; (2) the oxidized sapropel; (3) the active oxidation zone between the modern manganese and iron redox boundaries (Mn RB and Fe RB); (4) the sapropel; and (5) the synsapropel.

[6] The main original source of magnetic material throughout the entire box core has been eolian dust. The sediments at the top of the core, above the oxidized sapropel, have experienced only oxic conditions. Therefore the original single-domain (SD) to pseudo-single-domain (PSD) magnetic grain size of the eolian dust has been preserved. During formation of the sapropel the geochemical conditions were anoxic and sulfidic. Reductive diagenesis in the sapropel resulted in an increase of the magnetic grain size, because smaller grains are affected most. Also, bacterial sulfate reduction produced pyrite and possibly some magnetic iron sulfides. Since

the sapropel S1 has been buried below oxic sediments, oxidation of the sapropel has occurred, starting at the top. Iron oxides precipitate in the zone of active oxidation between the modern manganese redox boundary and the iron redox boundary. Amorphous Fe oxides age to form superparamagnetic (SP) grains. Moreover, new high-coercive magnetic material is formed, presumably magnetosomes. The zone of active oxidation has moved downward with time, so a progressively larger part of the original sapropel became oxidized. The SP content decreases to the top of the oxidized sapropel, which has been subjected to oxic conditions for the longest time, as SP material ages to larger grains. In the oxidized sapropel the median destructive fields of IRM and anhysteretic remanent magnetization (ARM) increase downward to high values, suggesting a gradual downward increase in high-coercivity material. Also, the ARM/IRM ratio and the ratio of ARM (normalized by the DC bias field) over the initial magnetic susceptibility ( $\chi_{\text{ARM}}/\chi_{\text{in}}$ ) show a peak in the oxidized sapropel and in the active oxidation zone. However, the  $S$  ratio remains high in the oxidized sapropel, suggesting a dominance of low-coercivity material. Only in the active oxidation zone the  $S$  ratio drops to lower values and recovers to high values in the sapropel. This  $S$  ratio behavior cannot be explained by the occurrence of high-coercive material both in oxidized sapropel and in the zone of active oxidation.

## 3. Methods

### 3.1. Samples

[7] In this study we analyze box core ABC26 with new methods. Box core ABC26 (30 cm long) was recovered 200 km south of Crete (33°21.3'N, 24°55.7'E, water depth 2150 m, Figure 1) during the 1987 ABC expedition of

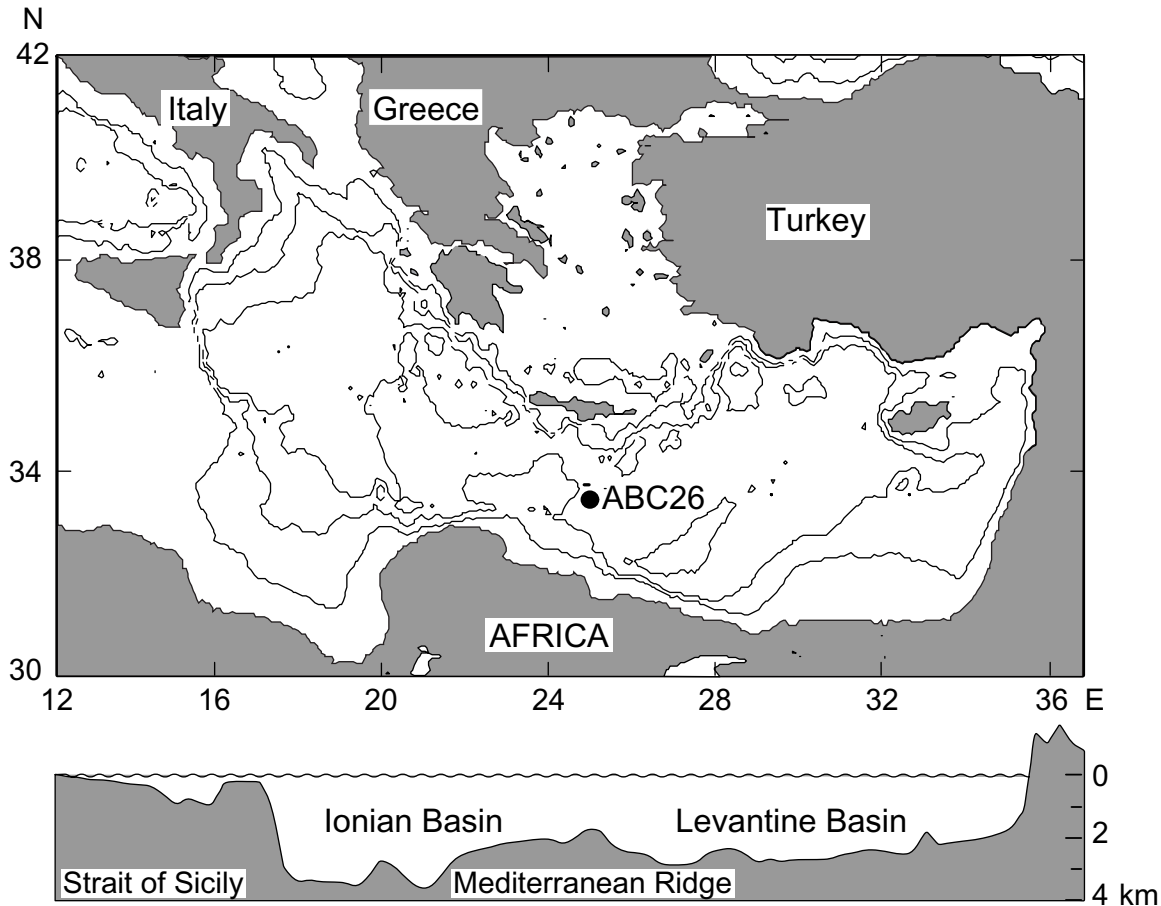


**Figure 1.** Location map of box core ABC26 in the eastern Mediterranean Sea.

R/V *Tyro*. Subcores were stored at 4°C and subsampled at a resolution of 3 mm. The sediment was dried in a stove at 60°C and pulverized in an agate mortar. About 100 mg of each sample were weighed into 8 mm<sup>3</sup> cylindrical vials and molded into epoxy resin (Ciba-Geigi Araldite D/Hardener HY926; no accelerator was used) until a homogeneous dispersion was obtained. The hardening took 24 hours at room temperature and was done in a low-field environment. Twenty-nine samples with an average down core sample spacing of 1 cm were prepared for IRM analyses. A sample vial containing epoxy resin has been

included in the analysis as a blank to provide a correction for the small IRM contribution of the epoxy resin and the vials.

### 3.2. IRM Component Analysis

[8] *Kruiver et al.* [2001] developed a method to analyze IRM acquisition curves on the basis of the cumulative log-Gaussian appearance of such curves. Provided that magnetic interaction is absent, each component in a magnetic mineral assemblage can be characterized by (2) its saturation IRM (SIRM); (2) the field at which half of the SIRM is reached,  $B_{1/2}$ , and (3) the

dispersion of the distribution, DP. Measured IRM data are fitted by forward modeling of a user-specified number of components. Data are fitted in three different representations of the acquisition data (abscissa always log-transformed): (1) on a linear ordinate (linear acquisition plot (LAP)), (2) as a gradient curve (gradient acquisition plot (GAP)) and (3) on a standardized ordinate (standardized acquisition plot (SAP)). The fit is optimized by minimizing the sum of the squared residuals for the three different plots. In case of doubt on the number of components or optimal parameters,  $F$  test and  $t$  test statistics are applied to the residuals to facilitate the decision on the best fit.

[9] Stepwise IRM acquisition was applied with a PM4 pulse magnetizer in 27 field steps, ranging from 5 mT up to 2.5 T. The steps were approximately equidistant on a log-scale. Note that quoted  $^{10}\log(B_{1/2})$  and DP values have units of  $^{10}\log(\text{mT})$ . The blank sample acquired a weak IRM:  $\text{SIRM} = 2.86 \times 10^{-8} \text{ Am}^2$  per sample vial,  $^{10}\log(B_{1/2}) = 1.53$  ( $B_{1/2} = 34 \text{ mT}$ ), and  $\text{DP} = 0.39$ . The IRM acquisition curves were corrected for the epoxy resin contribution by including a fixed component in the analysis with characteristics specified above.

### 3.3. Hysteresis Measurements

[10] For five selected samples (one in each geochemical zone) hysteresis curves and FORC diagrams [Pike *et al.*, 1999; Roberts *et al.*, 2000] were determined. Ten to thirty milligrams of sample powder were homogeneously dispersed into tiny epoxy resin cylinders ( $\emptyset$  3 mm, length 4–5 mm). Measurements were performed on an alternating gradient magnetometer (MicroMag, Princeton) with a P1 phenolic probe. The sample cylinders were glued to the probe to minimize noise due to movement of the cylinder relative to the

probe. Because of partial saturation of the pole shoes, the response of the MicroMag is not linear for fields larger than 1.6 T. Therefore we applied maximum fields of 1.6 T in all cases. For the hysteresis curves, the averaging time for each data point was 0.1 s; field increments were 10 mT. Backfield curves allowed for the determination of  $B_{\text{cr}}$  after an applied positive field of 1.6 T.

[11] FORC diagrams were measured for these five selected samples [Pike *et al.*, 1999; Roberts *et al.*, 2000]. First, a large positive field is applied and ramped down to the reversal field  $B_a$ . Then, the magnetization is measured as the field  $B_b$  is increased from  $B_a$  back up to saturation. A mixed second derivative of the magnetization to  $B_a$  and  $B_b$  defines the FORC distribution. It is convenient to apply a change of coordinates to  $B_u$  ( $\equiv (B_a + B_b)/2$ ) and  $B_c$  ( $\equiv (B_b - B_a)/2$ ). In this way,  $B_c$  may be interpreted as particle coercivity and  $B_u$  to the local interaction field. A smoothing factor (SF) is applied to suppress noise in the contours of the FORC diagram. The pattern of contours in a FORC diagram is indicative of superparamagnetic, (pseudo)single-domain or multidomain behavior, whereas deviations from the  $B_u = 0$  axes indicate magnetic interaction [Pike *et al.*, 1999; Roberts *et al.*, 2000].

[12] For each FORC diagram, 150 reversal curves were measured with an averaging time of 0.5 s per data point. We needed to measure during the night to minimize background noise. Three runs per sample were performed: (1) focus on very low  $B_c$  values to detect SP magnetite:  $B_c$  ranges 0–25 mT and  $-50 \text{ mT} \leq B_u \leq 50 \text{ mT}$ ; (2) focus on low  $B_c$  values to detect SD magnetite:  $B_c$  ranges 0–80 mT and  $-100 \text{ mT} \leq B_u \leq 100 \text{ mT}$ ; and (3) focus on higher  $B_c$  values to detect hematite:  $B_c$  ranges 0–400 mT and  $-60 \text{ mT} \leq B_u \leq 60 \text{ mT}$ .

## 4. Results

### 4.1. IRM Components

[13] A prerequisite for the applicability of the IRM component analysis is the absence of magnetic interaction. For these ABC26 sediments this prerequisite is checked by FORC analyses (see section 4.2). Magnetic interaction is not detected in these samples. Additionally, *Robertson and France* [1994] showed that magnetic interaction affects the IRM acquisition curve only when the grains are almost touching. In our samples this is not the case, because the powders were dispersed in epoxy resin. Therefore IRM component analyses can be applied.

[14] Examples of IRM component analyses are given in Figure 2, for which the fitted IRM components are given in Table 1. The dotted line represents the blank of epoxy resin contribution, which is generally 5–10% of the total SIRM. In the following analyses, the contribution of the epoxy resin has been corrected for.

[15] Two magnetic components are invariably present in the core (Figure 2): a relatively strong low-coercivity component (component 1) and a relatively weak high-coercivity component (component 2). Component 1 is magnetite that was recognized in earlier studies [*Passier et al.*, 2001; *Passier and Dekkers*, submitted manuscript, 2001]. Component 2, likely hematite, was not detected before. For a good fit of the IRM data this hematite component must be included, even with an average contribution of only 6% to the total SIRM.

[16] Both in the oxidized part of the sapropel and in the zone of active oxidation, the magnetite (Figure 2b) and hematite (Figure 2c) components are common as well. However, an additional coercivity component (component 3)

is present in these zones. It is evidently present in the data displayed as GAPs and SAPs but not so obvious in the LAPs, an indication that for a proper interpretation all three plots are necessary. For the samples in the oxidized zones both three- and two-component fits (apart from the epoxy contribution) are determined.  $F$  and  $t$  test statistics is used to determine the better of the two fits [*Kruiver et al.*, 2001]. Two examples of the  $F$  and  $t$  tests are given in Table 2 for the samples displayed in Figures 2b and 2c. For sample 77924 from the oxidized sapropel, the  $F$  values are higher than the critical  $F$  value (1.9) for all three representations of the data. This indicates that the three-component fit (fit 1) is better than the two-component fit (fit 2) on a 95% confidence level. For sample 77935 both LAP and SAP are statistically better for the three-component model. The  $F$  value for the GAP is lower than the critical  $F$ , as is the  $t$  value. Thus the two- and three-component fits are equally good for the GAP from a statistical point of view. However, because the LAP and SAP statistics indicate that fit 1 is better, the three-component model is favored for sample 77935.

[17] The down core  $S$  ratio is shown in Figure 5f: it is high in the top sediment, slightly higher in the oxidized sapropel, a significant drop in the active oxidation zone, and a recovery to high values in the sapropel and synsapropel. There is a good agreement between the measured  $S$  ratio with a forward field (this study) and the measured  $S$  ratio with a backfield [*Passier et al.*, 2001]. The down core patterns are identical, but in the extreme zone of active oxidation their absolute values differ (up to 13%). This difference may be related to interaction that can slightly affect IRM analyses [*Robertson and France*, 1994], although it was not detected by FORC analysis (section 4.2). However, some magnetic interaction could occur in samples with magnetosomes, because these magnetite crystals

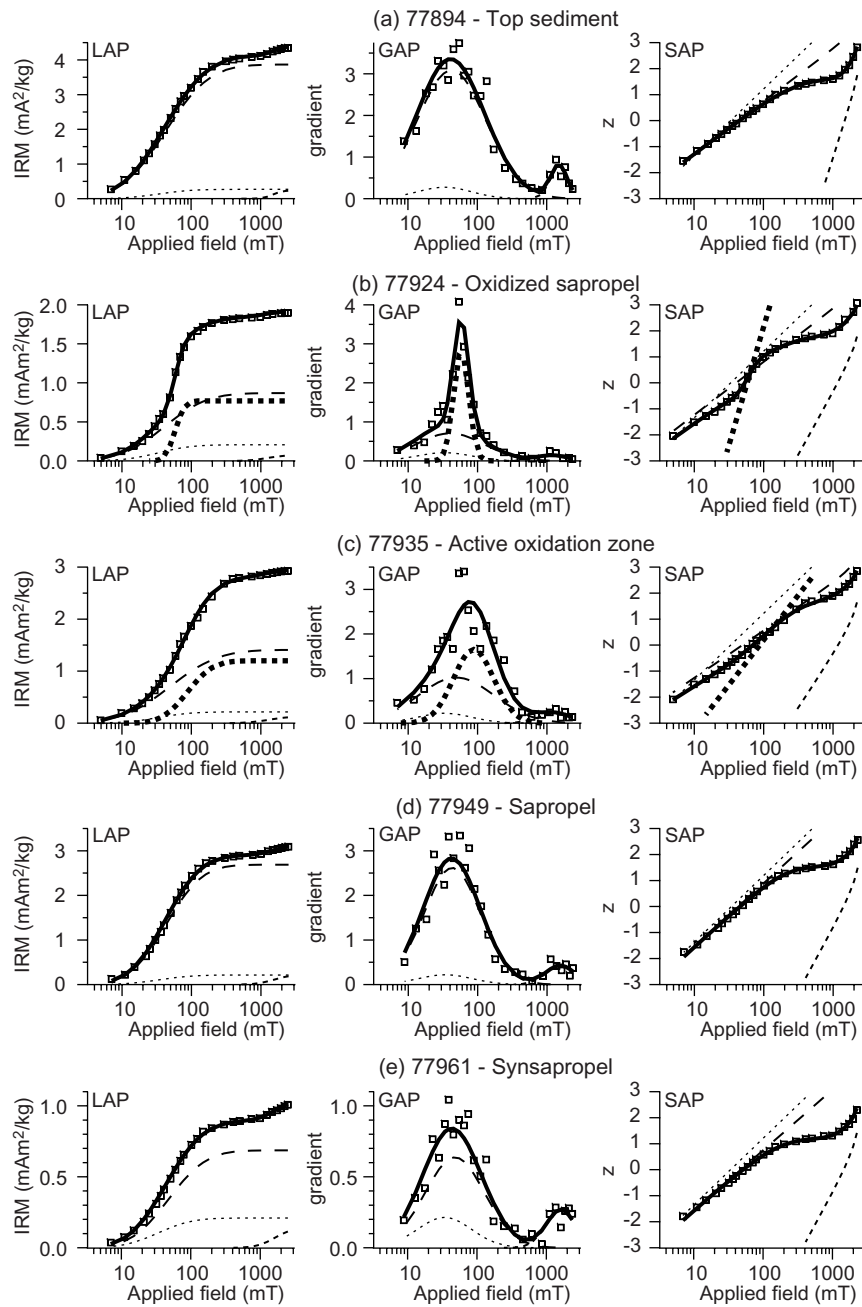


**Figure 2.** Examples of IRM component analyses: LAP, GAP, and SAP for (a) 77894, top sediment; (b) 77924, oxidized sapropel; (c) 77935, active oxidation zone; (d) 77949, sapropel; and (e) 77961, synsapropel. Squares, data points; thin dotted line, epoxy resin contribution; long dash, component 1; short dash, component 2; thick short dash, component 3; thick solid line, sum of the individual components.

**Table 1.** Parameter Values of IRM Coercivity Components<sup>a</sup>

Sample	Zone	Epoxy Resin			Component 1			Component 2			Component 3		
		SIRM	log ( $B_{1/2}$ )	DP	SIRM	log ( $B_{1/2}$ )	DP	SIRM	log ( $B_{1/2}$ )	DP	SIRM	log ( $B_{1/2}$ )	DP
77894	top sediment	0.271	1.53	0.39	3.87	1.63	0.51	0.24	3.18	0.12			
77924	oxidized sapropel	0.208	1.53	0.39	0.87	1.61	0.49	0.074	3.09	0.21	0.77	1.77	0.11
77935	active oxidation zone	0.218	1.53	0.39	1.41	1.7	0.55	0.13	3.12	0.25	1.2	1.95	0.29
77949	sapropel	0.216	1.53	0.39	2.69	1.63	0.41	0.226	3.19	0.21			
77961	Synsapropel	0.21	1.53	0.39	0.687	1.68	0.43	0.141	3.21	0.21			

<sup>a</sup>Units for SIRM are  $\text{mAm}^2/\text{kg}$ ; units for  $^{10}\log(B_{1/2})$  and DP are  $^{10}\log(\text{mT})$ .

occur in chains [Moskowitz, 1993]. Sample handling, however, probably caused disruption of most of the chains. Moreover, the powdered sample was dispersed evenly in the epoxy resin, and hence the grains are not touching. In section 5.3.3 we explain the trends in  $S$  ratio in terms of properties of the magnetic components.

#### 4.2. Hysteresis and FORC Diagrams

[18] Representative hysteresis curves are shown in Figure 3. The curves were measured up to 1.6 T, but only the central segment between  $\pm 300$  mT is shown for clarity. The curves are saturated for fields of 1.6 T. However, they are not closed in fields of 300 mT, which indicates the presence of a high-coercive mineral identified as component 2 in the IRM analysis. The hysteresis curves mostly show the same features as observed in the earlier study of ABC26 [Passier *et al.*, 2001]. The parallel branches in sample 77894 from the top sediments indicate a mixture of SD and some SP magnetite, corresponding to IRM component 1. It is not likely that MD magnetite is present, because of the high  $B_c$  and  $B_{cr}$  values. Sample 77924 from the oxidized sapropel layer, however, displays a potbelly curve, indicating a mixture of SD

and a lesser amount of SP magnetite [Tauxe *et al.*, 1996]. On the other hand, sample 77938 from the active oxidation front is slightly wasp-waisted, suggesting a mixture of SP and very coercive SD magnetite, probably IRM component 3.

[19] Hysteresis parameters for these curves are given in Table 3. It should be noted, however, that values of  $B_c$  and  $B_{cr}$  are not representative of the magnetite in the samples, since all samples contain mixtures of two or three magnetic minerals, including hematite. However, the hematite contribution is relatively small for  $B_c$ . The value of  $B_{cr}$  is more affected by the presence of hematite. The fact that  $B_c$  and  $B_{cr}$  do not describe either the dust magnetite or the additional magnetite in the oxidized zones is reflected in the absence of a correlation between  $B_{1/2}$  values of either component 1 or 2 and the hysteresis  $B_c$  and  $B_{cr}$  values in these zones. However, the general pattern of  $B_{1/2}$  of component 1 and  $B_{cr}$  seems to correlate in the top sediment and in the (syn)sapropel, although their values are not identical.

[20] The magnetic domain state and magnetic mineral content is further investigated using FORC diagrams (Figure 4). In all diagrams, contour lines end more or less perpendicular to

**Table 2.** Examples of  $F$  and  $t$  Test Statistics for Either a Three- or a Two-component Fit for the Samples From the Oxidized Zones<sup>a</sup>

77924					77935								
Component	SIRM	log( $B_{1/2}$ )	DP	Residuals			Component	SIRM	log( $B_{1/2}$ )	DP	Residuals		
				LAP	GAP	SAP					LAP	GAP	SAP
Fit 1				0.0104	1.30	0.0702					0.0333	3.13	0.062
epoxy	0.208	1.53	0.39				epoxy	0.218	1.53	0.39			
1	0.87	1.61	0.49				1	1.41	1.70	0.55			
2	0.074	3.09	0.21				2	0.13	3.12	0.25			
3	0.77	1.77	0.11				3	1.20	1.95	0.29			
Fit 2				0.187	8.44	0.753					0.0183	3.90	0.289
epoxy	0.208	1.53	0.39				epoxy	0.128	1.53	0.39			
1	1.63	1.67	0.38				1	2.63	1.80	0.48			
2	0.072	3.09	0.20				2	0.119	3.11	0.26			
Test Statistics	$F$ Test	Test Results					Test Statistics	$F$ test	$T$ test	Test Results			
LAP	1426	Fit 1 better					LAP	25		Fit 1 better			
GAP	147	Fit 1 better					GAP	1.52	0.42	No difference			
SAP	85	Fit 1 better					SAP	15		Fit 1 better			

<sup>a</sup>Units for SIRM are  $\text{mA m}^2/\text{kg}$ ; units for  $^{10}\log(B_{1/2})$  and DP are  $^{10}\log(\text{mT})$ . Critical  $F$  value on 95% confidence level for  $N = 26$  is 1.9; critical  $t$  value for  $N = 52$  is 1.7.

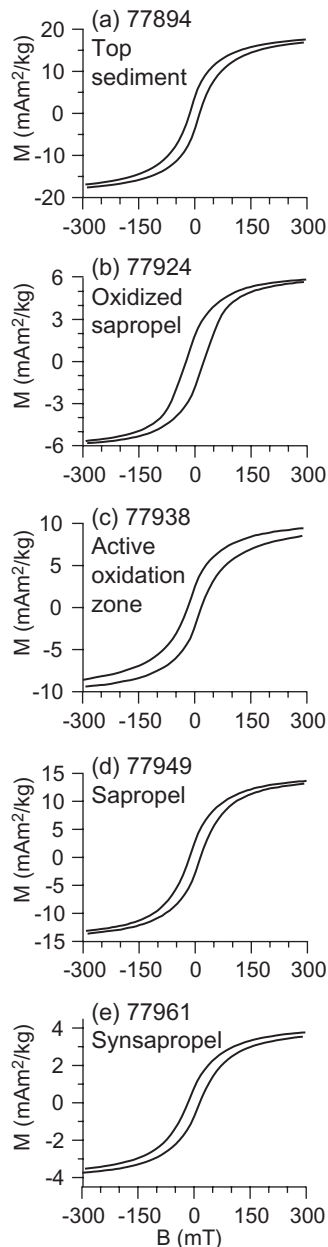


**Figure 3.** Hysteresis curves for five samples, one from each geochemical zone: (a) 77894, top sediment; (b) 77924, oxidized sapropel; (c) 77938, active oxidation zone; (d) 77949, sapropel; and (e) 77961, synsapropel. Curves were measured for  $-1.6 \text{ T} \leq B \leq 1.6 \text{ T}$  but are shown up to  $\pm 300$  mT. See method section for measurement settings.

the  $B_u$  axis at low  $B_c$ . For multidomain (MD) magnetite, contour lines would run parallel to the  $B_u$  axis. Therefore no MD magnetite is present in these samples. Furthermore, peaks are centered along the  $B_u = 0$  axis, and they show a narrow distribution along the  $B_u$  axis. This means that there is no detectable magnetic interaction [Pike *et al.*, 1999]. Therefore the prerequisite for the IRM component analysis of no magnetic interaction is met.

[21] The presence of both magnetite and hematite is evident for the unaffected magnetic material in the top sediment (Figure 4a): A peak in the low-coercivity range represents magnetite, and a tail to higher coercivities demonstrates the presence of hematite. The hematite contour lines are visible as a band to higher  $B_c$  in the high-coercivity panel. However, no structure (e.g., coercivity peak) can be observed in the hematite band, because of the magnetic dominance of magnetite over hematite in these samples. In the low-coercivity zoom panel the contour lines are almost closed at low  $B_c$ , indicative of the presence of some SP magnetite. The FORC of the sapropel (Figure 4c) is similar to the top sediment: both magnetite and hematite are detected. For this sample, contour lines are closed at low  $B_c$ , indicating SD behavior of the magnetite. The center of the magnetite peak is shifted to the right for the sapropel sample relative to the top sediment, indicating a slightly harder magnetite. This is supported by the higher hysteresis  $B_c$  for the sapropel (Table 3).

[22] A striking difference in appearance of the FORC diagrams emerges for the oxidized sapropel (Figure 4b). There is a pronounced magnetite coercivity peak, which occurs at much higher  $B_c$  ( $\sim 55$  mT). Moreover, this peak is asymmetrical in the  $B_c$  direction and smeared to lower  $B_c$  values. The peak centered at  $\sim 55$  mT is interpreted as the additional magnetite of component 3, while the

**Table 3.** Hysteresis Parameters for Representative Samples From the Five Geochemical Zones<sup>a</sup>

Sample	Zone	Depth, mm	$B_{cr}$ (mT)	$B_c$ (mT)	$B_{cr}/B_c$	$M_r$ (mAm <sup>2</sup> /kg)	$M_s$ (mAm <sup>2</sup> /kg)	$M_r/M_s$
77894	top sediment	76.4	37.5	13.1	2.86	3.796	19.15	0.20
77924	oxidized sapropel	168.6	49.5	23.5	2.11	1.851	6.267	0.30
77938	active oxidation zone	212.9	58.4	17.9	3.26	2.386	10.49	0.23
77949	sapropel	246.5	39.7	14.5	2.74	2.856	14.69	0.19
77961	synsapropel	283.4	45.3	15.8	2.87	0.769	4.122	0.19

<sup>a</sup> $M_s$ , saturation magnetization;  $M_r$ , saturation remanence;  $B_c$ , coercive force;  $B_{cr}$ , coercivity of remanence.

tail to lower  $B_c$  represents magnetite of component 1. Again, a hematite contribution is evident.

## 5. Discussion

### 5.1. Down Core Variations in Magnetic Components

[23] Component 1 is magnetite and constitutes the largest part of the SIRM. It was detected in earlier studies [Passier *et al.*, 2001]. The pattern of the SIRM<sub>1</sub> follows the pattern of eolian dust input, and therefore this magnetite is probably of eolian origin [Passier *et al.*, 2001]. The down core variations in SIRM for components 1 and 2 (presumably hematite) exhibit approximately the same patterns (Figures 5a and 5b). This suggests that the source of component 2 was also eolian dust that had a relatively uniform composition through time. SIRM<sub>2</sub>, however, is an order of magnitude lower than SIRM<sub>1</sub>. In earlier studies the presence of hematite in eolian dust has been observed as well [Walden and White, 1997; Frederichs *et al.*, 1999; Schmidt *et al.*, 1999]. The presence of hematite does not change the original geochemical-magnetic model for the processes around sapropel formation and burial [Passier *et al.*, 2001; Passier and Dekkers, submitted manuscript, 2001]. The SIRM of component 3 is in the same order of magnitude as component 1. However, it follows an entirely different pattern, suggesting that the

source of component 3 is different from the eolian dust.

[24] The ratio SIRM<sub>2</sub>/SIRM<sub>1</sub> is constant in the top sediment and varies slightly in the sediment zones that have been affected by reductive diagenesis. In the synsapropel the ratio SIRM<sub>2</sub>/SIRM<sub>1</sub> is elevated, indicating a higher sensitivity to redox conditions of magnetite relative to hematite. This observation appears to be contrary to those of Canfield *et al.* [1992], who found that hematite is more reactive toward sulfide than magnetite. However, Canfield *et al.* [1992] determined the reaction rate of synthetic hematite with varying concentrations of sulfide solutions in the laboratory, which might not be representative of hematite in eolian dust or conditions in and near the sapropel. Moreover, in eolian dust, hematite may be present not only as accessible grains or coatings but also as inclusions in silicate minerals that are protected against reductive dissolution [Walden and White, 1997].

[25] The mean coercivity of component 1 is nearly constant down core (Figure 5c) but is elevated in the active oxidation zone (56 versus 45 mT on average). Also, the dispersion is relatively large in this zone. Component 3 is distinctly harder (average of 68 mT) than component 1 and exhibits a very narrow dispersion (0.18 versus 0.51). The small DP suggests that the grain size range of the additional magnetite is narrow. Component 3 has

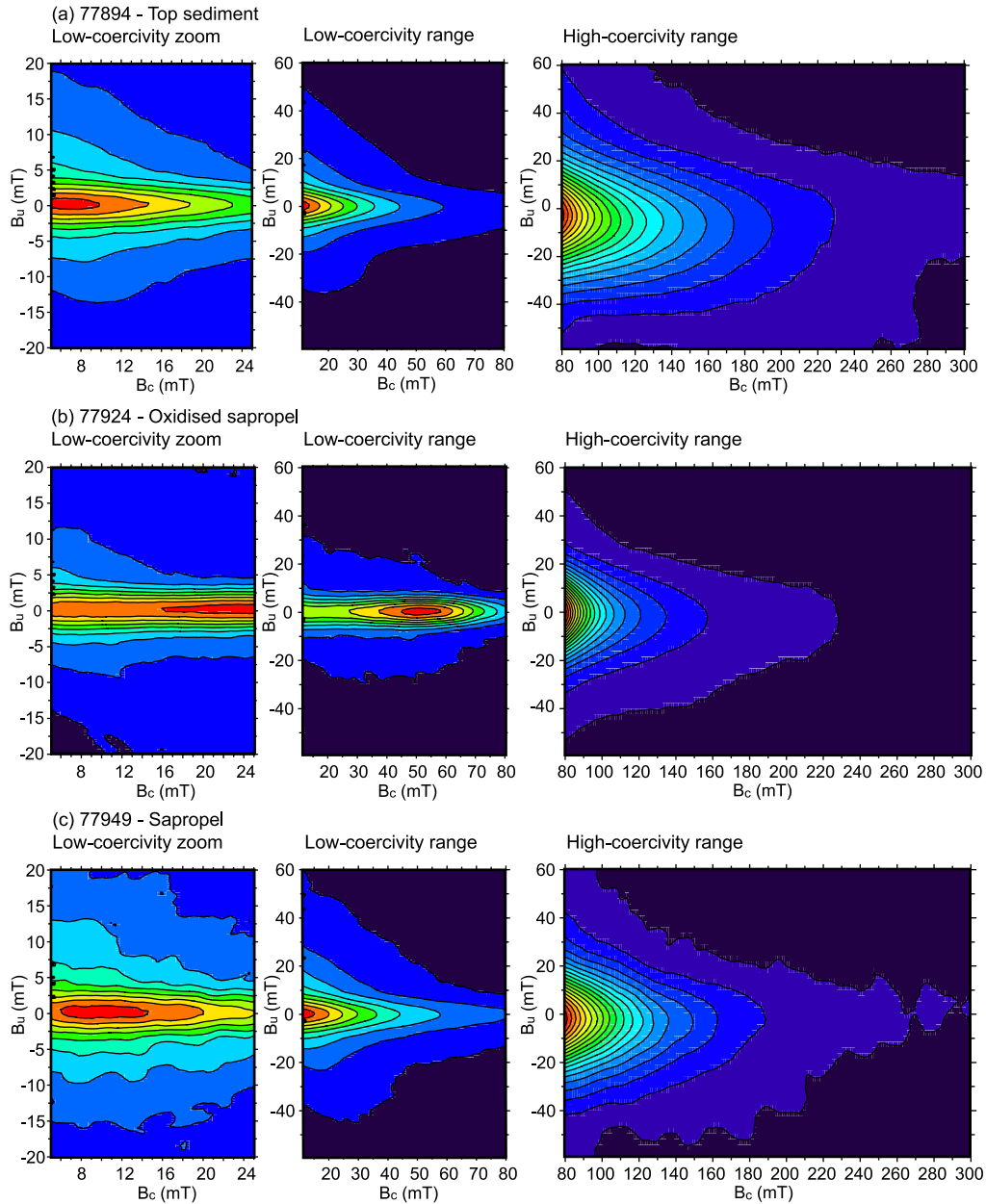


**Figure 4.** Representative FORC diagrams: (a) 77894, top sediment; (b) 77924, oxidized sapropel; and (c) 77949, sapropel. From left to right are shown magnetite range with very low coercivity zoom, SF = 5, 10 contours; magnetite range coercivities, SF = 5, 10 contours; and hematite range coercivities, SF = 8, 20 contours. Each diagram is normalized by its maximum value. See section 3 for measurement settings.

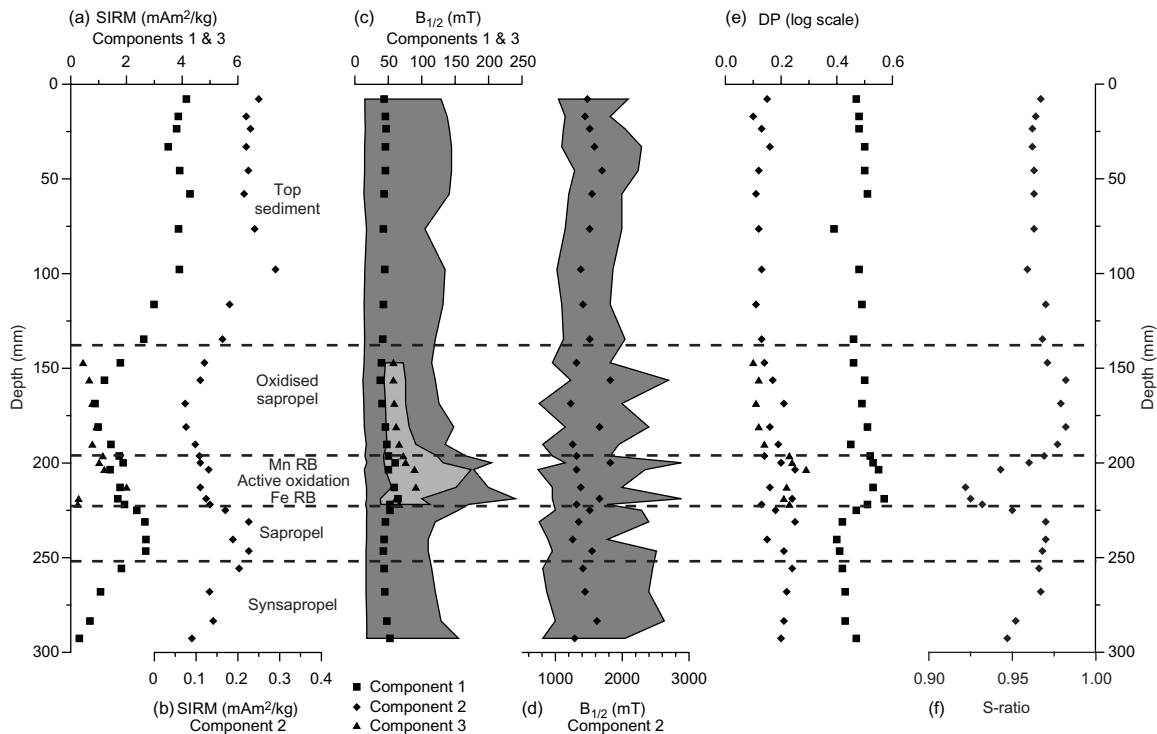


**Figure 5.** Down core variations in IRM parameters. SIRM for (a) components 1 and 3 (both magnetites) and (b) component 2 (hematite). Note the different order of magnitude in SIRM in Figures 5a and 5b. Squares, component 1; diamonds, component 2; triangles, component 3. Mean coercivity  $B_{1/2}$  on a linear scale for (c) components 1 and 3 and (d) component 2. The shaded area around the mean coercivity denotes one standard deviation, the dispersion of the distribution DP. Symbols are as in Figures 5a and 5b. (e) DP on a log scale for components 1, 2, and 3. Symbols are as in Figures 5a and 5b. (f) Forward measured  $S$  ratio for ABC26 (300 mT field combined with a 1 T field according to equation (4)). Dashed horizontal lines indicate the boundaries of different geochemical zones in the core. Fe RB, modern iron redox boundary; Mn RB, modern manganese redox boundary.

higher dispersions in the active oxidation zone relative to the oxidized sapropel (0.24 versus 0.12), but DPs are still low compared to those of the original eolian magnetite.

[26] When the three IRM parameters (SIRM,  $\log(B_{1/2})$ , and DP) are plotted in three dimensions (Figure 6), the three magnetic components appear to be grouped into separate clusters. Although the mean coercivity of component 1 seems to be almost constant when plotted down core, the different geochemical zones yield distinct groups in three dimensions.

The top sediment samples plot in a different region than the samples that have undergone reductive diagenesis during some time of their history. However, even among these samples that have all undergone a different succession and degree of reductive diagenesis and oxidation, groups can be distinguished for component 1 that coincide with the redox layers. Although grouping of IRM parameters corresponding to geochemical zones is clear for components 1 and 3, this grouping is less evident for the hematite component (component 2). This indicates that hematite probably

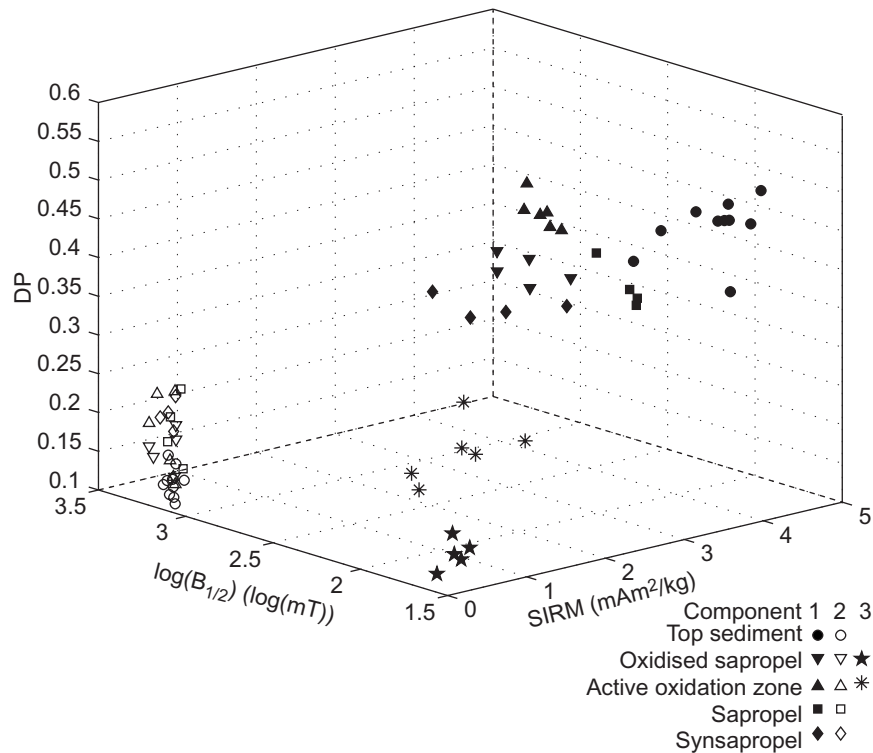


**Figure 6.** Three-dimensional representation of the IRM component data. Samples from different geochemical zones are clustered for components 1 and 3. Clustering for component 2 is not evident. See legend for symbols.

was not affected by these diagenetic processes to the same extent as magnetite.

[27] In these complex environments, where reductive diagenesis is followed by oxidation in some parts of the sediments, it is imperative to interpret variations in IRM parameters through time, rather than with depth in the core. The top sediment represents magnetic material unaffected by either reductive diagenesis or oxidation. During sapropel formation the symsapropel and the sapropel experienced reductive diagenesis, causing a slight drop in DP. After sapropel formation had ceased, oxidation of the top of the sapropel caused an increase in the coercivity of the originally eolian magnetite (component 1) in the oxidized zones relative to the sapropel and

the symsapropel. Moreover, component 3 began to form.

## 5.2. Magnetosomes

[28] Earlier studies suggested that the extra magnetic component in the oxidized sapropel and in the active oxidation zone consists of magnetosomes produced by magnetotactic bacteria [Passier *et al.*, 2001; Passier and Dekkers, submitted manuscript, 2001]. This study shows that the extra component in this zone (component 3) has very specific coercivity characterizations. It has a high coercivity for magnetite and a very low dispersion in comparison to the dust magnetite. The latter suggests a narrow grain size range, which is a strong indication for magnetosomes as the constituents of the

additional magnetite [Moskowitz *et al.*, 1989; Bazylinski, 1996]. In addition, the DP of the additional magnetite is lower in the oxidized sapropel than in the active oxidation zone. This suggests that as the extra magnetite becomes older (when the active oxidation front moves down in the sapropel), its grain size becomes more confined. This may be related to the presence of more living bacteria in the active oxidation zone, as the magnetotactic bacteria preferentially live in a transition zone from oxic to suboxic sediments. During the formation process of the magnetosomes a range of grain sizes is present inside the bacterial cells, resulting in a higher DP. When the magnetosomes are in the process of formation, the SIRM values are lowest: just above the Fe redox boundary. After the death of the magnetosome-containing bacteria, recrystallization confines the grain size to a smaller DP. The coercivity of the magnetosomes is rather high (average of 68 mT) compared to the range specified by Moskowitz [1993], which is 50 mT for whole-cell magnetosomes and 35 mT for extracted magnetosomes.

### 5.3. *S* Ratio

#### 5.3.1. Investigation of the *S* ratio

[29] The *S* ratio has been defined to describe the relative contributions of high-coercive to low-coercive magnetic phases. We assess the existing formula for the *S* ratio to include it in our model analysis to study the effects of varying coercivity characteristics on the value of the *S* ratio. The *S* ratio can be defined as the inverse of the ratio of the IRM intensity at any high field over the IRM intensity at any low backfield to quantify how much of the low-coercivity material is remagnetized by the backfield. Generally, the high field is taken at 1 T, and the  $IRM_{1T}$  is assumed to be the SIRM. The backfield is usually 0.3 T, because that field strength generally saturates magnetite. The classical *S*

ratio is given by [Thompson and Oldfield, 1986]

$$S_{\text{classic}} = -\left(\frac{IRM_{-0.3T}}{SIRM_{1T}}\right). \quad (1)$$

[30] If only low-coercivity minerals such as magnetite are present, the *S* ratio should be equal to 1, because these minerals should be saturated by fields of 300 mT. When both high- and low-coercivity minerals are present, the *S* ratio drops to lower values. *S* ratio values defined in (1) range between  $-1$  and  $+1$ . If no magnetic interaction occurs, this classically defined *S* ratio can be rewritten as (Figure 7)

$$S_{\text{classic}} = \frac{2a}{b} - 1, \quad (2)$$

where *a* is the IRM intensity at a positive field of 300 mT and *b* is the IRM intensity at a positive field of at 1 T.

[31] Bloemendal *et al.* [1992] redefined the *S* ratio; then, varying between 0 and 1,

$$S_{\text{Bloemendal}} = \left[1 - \frac{IRM_{-0.3T}}{SIRM_{1T}}\right]/2. \quad (3)$$

[32] The Bloemendal *S* ratio definition is a more logical choice of definition than the classical definition. Moreover, the Bloemendal *S* ratio allows us straightforward modeling of the expected *S* ratio for a certain magnetic mineral assemblage, provided no magnetic interaction occurs. Rewritten, (3) conforms to

$$S_{\text{Bloemendal}} = a/b, \quad (4)$$

which is the IRM at 0.3 T during acquisition over the IRM at 1 T (Figure 7), also called the *S'*-ratio or the “forward” *S* ratio. We will continue to use the Bloemendal *S* ratio (called the *S* ratio from now on) instead of the classical one.

#### 5.3.2. Simulated *S* ratios for single magnetic minerals and mixtures

[33] Since the *S* ratio can be derived from the IRM acquisition curve, it can be modeled for

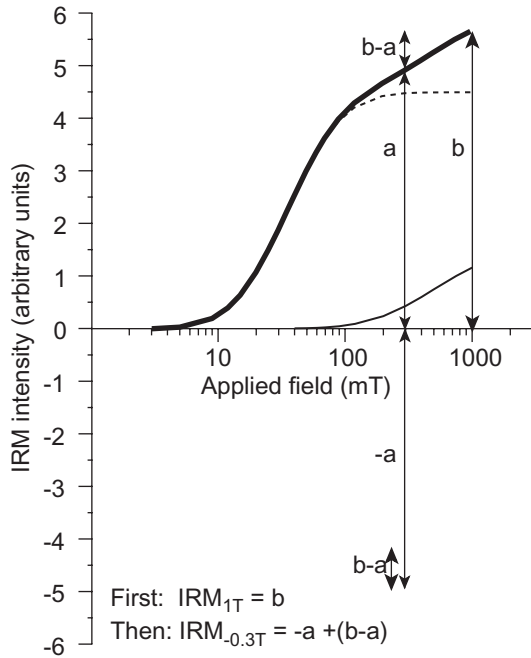


**Figure 7.** Schematic derivation of the  $S$  ratio. For a backfield  $S$  ratio, first a field of 1 T is applied, resulting in an IRM intensity of  $b$ . Subsequently, an opposite field of 300 mT redirects part of the magnetic mineral assemblage to  $-a$ , resulting in an IRM intensity of  $-a + (b - a)$ .

known IRM components using (4) on the total modeled IRM curve. We examine the effect of varying  $B_{1/2}$  and DP values for single magnetic minerals as well as for mixtures with varying relative contributions. We model theoretical magnetic mineral assemblages to investigate trends in the  $S$  ratio, and their coercivity characteristics are comparable to real magnetite, hematite, and goethite samples.

[34] Figure 8 shows the effect of varying mean coercivity for a single magnetic mineral when DP is fixed (Figure 8a) and the effect of varying DP when  $B_{1/2}$  is fixed (Figure 8b). Within the magnetite range, varying the mean coercivity at constant DP (Figure 8a) allows for

a theoretical range in  $S$  ratio values of a few percent from 1. Thus a drop in  $S$  ratio of several percent does not necessarily indicate addition of a high-coercivity mineral such as hematite, but this drop can be caused by variations in the magnetic properties of the magnetites itself, such as varying degrees of oxidation or titanium substitution. The effects are more dramatic for hematite and goethite. For fixed DP the  $S$  ratio varies between  $\sim 0.1$  and  $\sim 0.5$  for hematite.

[35] For increasing DP with fixed mean coercivity (Figure 8b) the  $S$  ratio drops slightly for magnetite. The drop is larger for harder magnetite with a larger DP, because the higher-field tail of the population is not saturated by fields of 300 mT, resulting in a lower estimate of the amount of low-coercivity material. For hematite and goethite the effect of increasing DP is opposite to that for magnetite. For a larger DP a larger part of the lower-field tail of the population is magnetized by the 300 mT field, and a larger part of the high-field tail is not saturated by the 1T field. These two effects induce an increase in the  $S$  ratio. The analyses of the  $S$  ratio for single magnetic minerals show that variations in mean coercivity and DP can have a profound effect on the  $S$  ratio.

[36]  $S$  ratio variations as a result of varying contributions in mixtures of two or three minerals are displayed in Figure 8c. Parameter values for the individual magnetic components are chosen to represent minerals that are found in the ABC26 sediments. The mixture of magnetite D (representative of the dust magnetite) and hematite allows for a classical interpretation of the  $S$  ratio: the  $S$  ratio drops when the contribution of the high-coercivity mineral relative to the low-coercivity mineral increases. This drop could also be explained by varying the hematite characteristics as sole mineral (Figure 8a) without the need of addition of

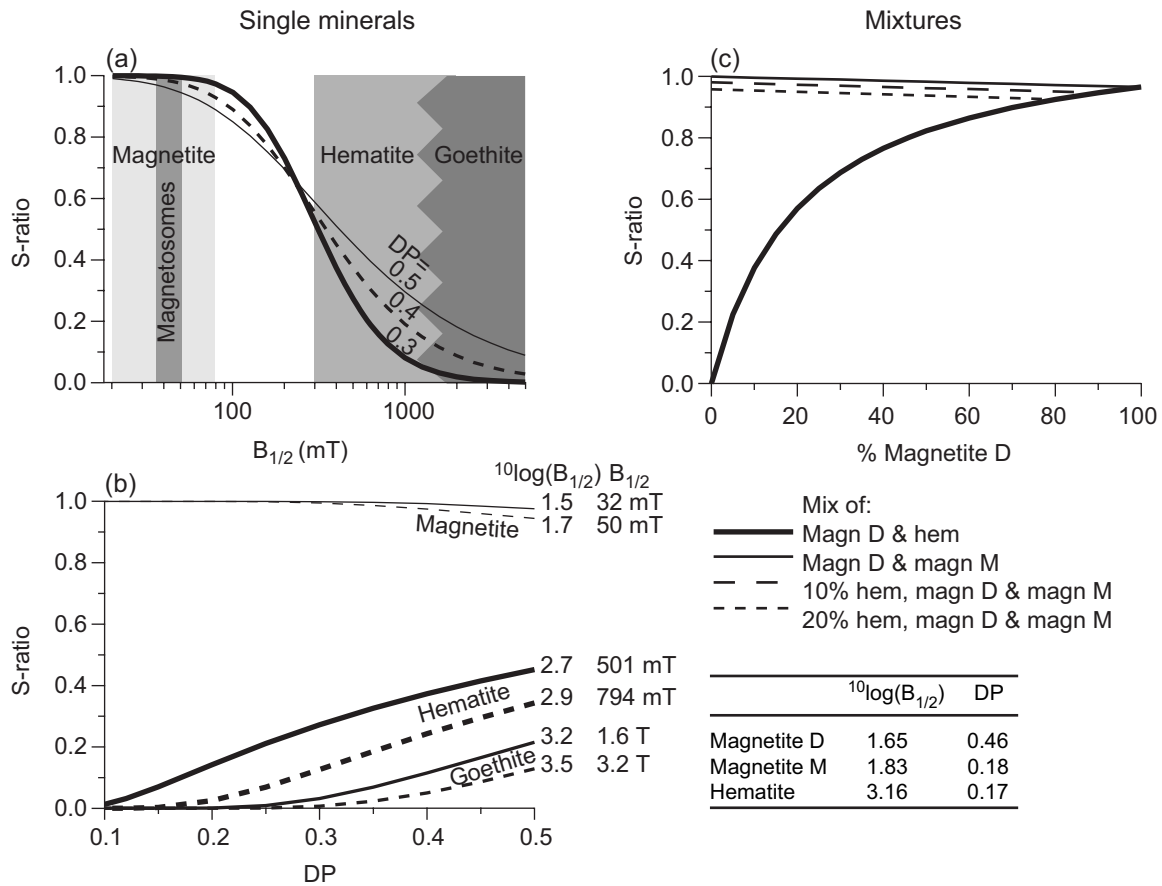


**Figure 8.** (a) Theoretical effect of varying mean coercivity with fixed DP on the  $S$  ratio for a modeled single magnetic mineral. Magnetite, hematite, and goethite regions are shaded. (b) Theoretical effect of varying DP with fixed mean coercivity on the  $S$  ratio for a modeled single magnetic mineral. (c) Theoretical variation of  $S$  ratio for mixtures of two (solid lines) or three (dashed lines) magnetic minerals of which the characteristics are given in the table (bottom right). Percentages of magnetite D are based on the relative contribution of the SIRM of magnetite D to the total SIRM.

magnetite D. As *Bloemendal et al.* [1992] already mentioned, substantial amounts of hematite are required to cause a drop of a few percent in the  $S$  ratio values. Nonetheless,  $S$  ratios close to 1 are often interpreted to represent magnetite only, while hematite might well be present. Therefore the interpretation of the  $S$  ratio is not unique.

[37] The mixture of the two magnetites gives rise to variations in  $S$  ratio in the same range as

for magnetite as a single mineral. For 100% of magnetite D, the  $S$  ratio is slightly lower than 1, because a small higher-field tail is not saturated by the 300 mT field. For 100% of magnetite M (representative of the magnetosomes) the  $S$  ratio equals 1. Although the coercivity is higher in this case, the very narrow distribution assures that this magnetite is fully saturated by the 300 mT field. Varying contributions of magnetite D and magnetite M follow the mixing line between the two extremes.

[38] The mixtures of three magnetic minerals are represented by the dashed lines in Figure 8c. The contributions of hematite are fixed at 10 and 20%, while the contributions of the two magnetites are allowed to vary. We observe that the  $S$  ratio mixing line of magnetite D and magnetite M is shifted toward lower values when hematite is added. Still, the variations in  $S$  ratio are in the same range as for magnetite as a sole magnetic mineral (Figure 8a). These considerations prominently show that interpretations of  $S$  ratios in terms of magnetite/hematite (or magnetite/goethite) ratios can be a gross simplification of the real situation.

### 5.3.3. $S$ ratios for core ABC26

[39] The down core variations in the forward  $S$  ratio for the ABC26 sediments are shown in Figure 5f: high  $S$  ratios are found everywhere, except in the active oxidation zone. To investigate whether we can explain the down core pattern in  $S$  ratios with the modeled IRM components, the measured forward  $S$  ratios are plotted on the theoretical forward  $S$  ratio curves for mixtures (Figure 9a). Percentages of the various magnetic components have been derived from their relative SIRM values from the IRM component analysis. Since the samples from the top sediment and the (syn)sapropel do not contain magnetite M, they plot close to the hematite-magnetite D mixing line. Samples from the oxidized sapropel plot between the mixing lines of both magnetites combined with 0 and with 10% hematite and closely follow the slope of the magnetite D-magnetite M mixing line. Samples from the active oxidation zone roughly follow this trend as well.

[40] There are many competing effects in the  $S$  ratio: not only do the relative contributions of various coercivity components affect the  $S$  ratio but also the mean coercivities and the dispersions of the distributions. To investigate the causes of the variations in the measured  $S$  ratio,

we plot the  $B_{1/2}$  and DP values of the three coercivity components for all samples in Figures 9b–9g. In the oxidized sapropel the two magnetites have opposite effects on the  $S$  ratio. The larger DP and slightly higher coercivity of component 1 cause a decrease in  $S$  ratio. The addition of a substantial amount (30–40%) of a higher-coercive phase with a small DP (component 3, Figures 9d and 9g), however, causes an increase in  $S$  ratio, as expected from Figure 8c. The net effect is a slight increase in  $S$  ratio, relative to the overlying top sediment.

[41] In the active oxidation zone, these two effects also compete. In the interval of the lowest  $S$ -ratios, however, the contribution of component 3 is much lower than in the oxidized sapropel ( $\sim 10\%$  versus 30–40%). Here the net effect is a decrease in the  $S$  ratio. Apparently, the effect of a larger DP and slightly higher  $B_{1/2}$  for component 1 is more important in this interval than the addition of component 3.

[42] In the zones of the core that contain only components 1 and 2, the variations in measured  $S$  ratio seem to be controlled by the coercivity of the magnetite component, combined with a large DP (Figures 9b and 9e): for a higher coercivity, a relatively smaller part of the distribution is saturated by a 300 mT field, which results in a lower  $S$  ratio. The DPs and coercivities of the hematite component do not seem to influence the measured  $S$  ratio (Figures 9c and 9f). Moreover, the relative contribution of high- versus low-coercivity material does not correlate with the  $S$  ratio.

[43] From the analysis of mixtures and the variations in  $S$  ratio for core ABC26, we conclude that the conventional interpretation of the  $S$  ratio is not suitable to describe relative contributions of high- versus low-coercivity phases for mixtures of more than two phases. In core ABC26 the  $S$  ratio rather depends on

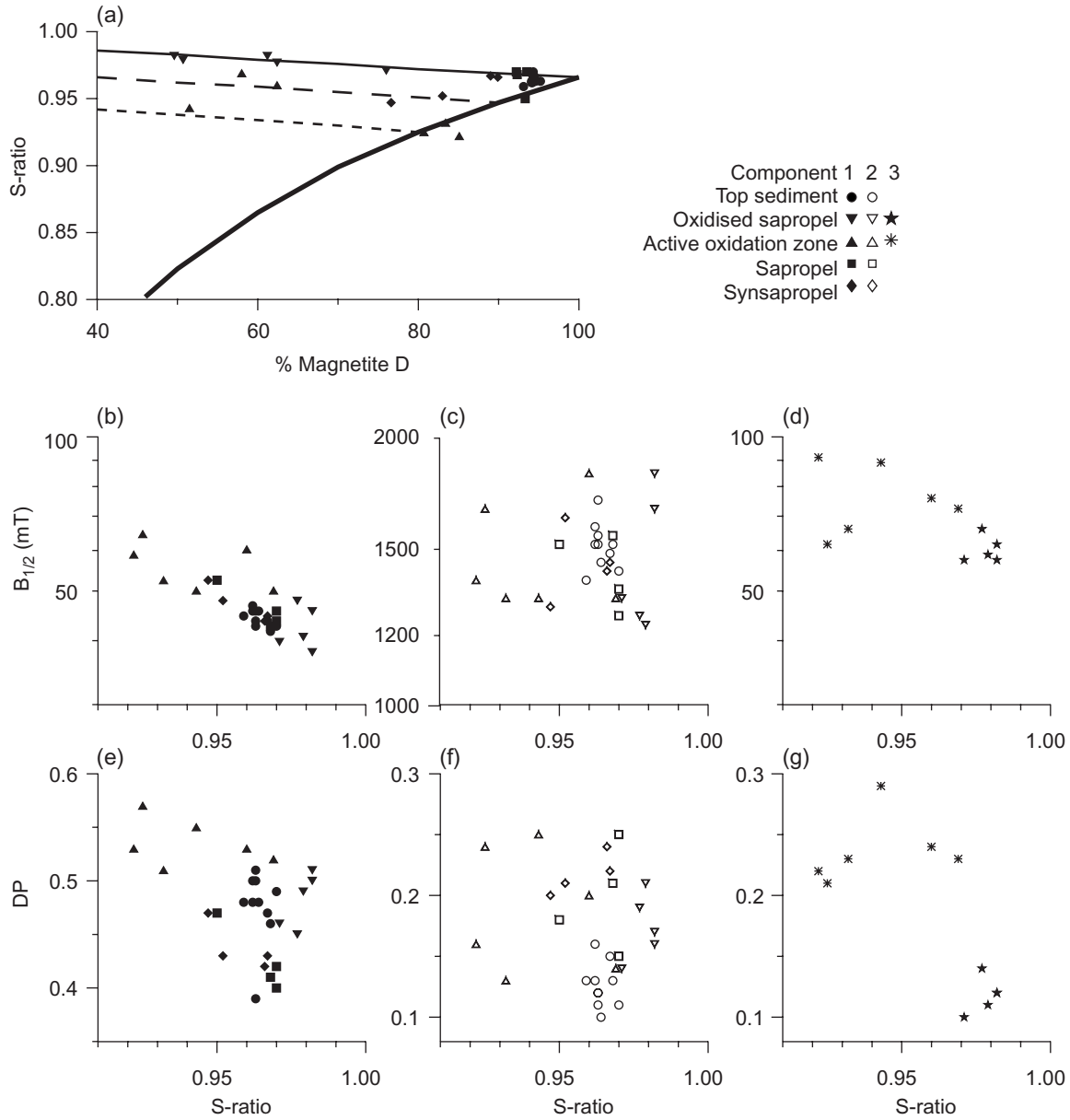


**Figure 9.** (a) Measured forward  $S$  ratios for ABC26 plotted with mixing lines of Figure 8c. Percentages of magnetite D are calculated using the ratio  $SIRM_1/SIRM_{total}$  from the IRM component analysis. Hematite content is generally between 4 and 10% of the total SIRM.  $B_{1/2}$  values (on a logarithmic scale) versus the measured forward  $S$  ratio for (b) component 1, (c) component 2, and (d) component 3. DP values versus the measured forward  $S$  ratio for (e) component 1, (f) component 2, and (g) component 3. See legend for symbols.

the coercivity characteristics of the individual coercivity components: their  $B_{1/2}$  and DP values. In the oxidized sapropel and in the active oxidation zone the  $S$  ratio responds differently to the presence of the third magnetic component, because of the different coercivity characteristics of both magnetites in these zones and their relative contributions. These dependencies explain why the down core profiles of coercivity measurements ( $B_c$ ,  $B_{cr}$ , and median destructive fields) and the down core profile of the  $S$  ratio [Passier *et al.*, 2001] do not have the same pattern. Therefore, in this case the  $S$  ratio cannot be diagnostic for the relative contribution of high-coercivity minerals (hematite) with respect to low-coercivity minerals (both magnetites).

## 6. Conclusions

[44] 1. The IRM component analyses showed that the input eolian dust consists of both magnetite and previously undetected hematite. The presence of hematite does not affect the original geochemical-magnetic model [Passier *et al.*, 2001; Passier and Dekkers, submitted manuscript, 2001].

[45] 2. An additional coercivity component is exclusively present in the oxidized sapropel and in the active oxidation zone. This magnetite component has a higher coercivity and a very small dispersion, suggesting a narrow grain size distribution. This is a strong indication that the extra magnetite phase consists of magnetosomes, which are formed in the active oxidation zone.

[46] 3. The FORC technique shows variations in magnetic mineral content and domain state that confirm the presence of the magnetic phases we found in the IRM component analyses. Moreover, magnetic interaction seems to be absent, which validates the use of the IRM component analysis.

[47] 4. The down core  $S$  ratio pattern can be explained by a mixture of two different magnetites and hematite in the oxidized sapropel and in the active oxidation zone and a mixture of magnetite and hematite in the rest of the core. The analysis shows that the  $S$  ratio is not diagnostic for the relative contributions of high- versus low-coercivity minerals for mixtures of more than two components. Rather, the  $S$  ratio depends on the mean coercivities and the DP values of the individual coercivity components. A theoretical investigation shows that even for single minerals the  $S$  ratio can vary significantly for varying mean coercivities or DPs. Therefore, although the  $S$  ratio is easily and quickly measured, its diagnostic value can be severely limited.

## Acknowledgments

[48] Valuable comments of Tom Mullender and Mark Dekkers and the journal reviewers Mike Jackson and Michael Urbat greatly improved the manuscript. This work is funded by the Netherlands Organization for Scientific Research (NWO/ALW). It is conducted under the program of the Vening Meinesz Research School of Geodynamics (VMSG). Samples are part of the EU-MAST program CT97-0137.

## References

- Bazylinski, D. A., Controlled biomineralization of magnetic minerals by magnetotactic bacteria, *Chem. Geol.*, *132*, 191–198, 1996.
- Bloemendal, J., J. W. King, F. R. Hall, and S.-J. Doh, Rock magnetism of Late Neogene and Pleistocene deep-sea sediments: Relationship to sediment source, diagenetic processes and sediment lithology, *J. Geophys. Res.*, *97*, 4361–4375, 1992.
- Canfield, D. E., R. Raiswell, and S. Bottrell, The reactivity of sedimentary iron minerals toward sulfide, *Am. J. Sci.*, *292*, 659–683, 1992.
- Emeis, K.-C., and Shipment Scientific Party, Paleoceanography and sapropel introduction, *Proc. Ocean Drill. Program Initial Rep.*, *160*, 21–28, 1996.
- Frederichs, T. W., U. Bleil, K. Däumler, T. Von Dobeneck, and A. M. Schmidt, The magnetic view on the marine paleoenvironment: Parameters, techniques, and potentials of rockmagnetic studies as a key to paleoclimatic

- and paleoceanographic changes, in *Use of Proxies in Paleoceanography: Examples From the South Atlantic*, edited by G. Fischer and G. Wefer, pp. 575–599, Springer-Verlag, New York, 1999.
- Haese, R. R., H. Petermann, L. Dittert, and H. D. Schulz, The early diagenesis of iron in pelagic sediments: A multidisciplinary approach, *Earth Planet. Sci. Lett.*, *157*, 233–248, 1998.
- Kruiver, P. P., M. J. Dekkers, and D. Heslop, Quantification of magnetic coercivity components by the analysis of acquisition curves of isothermal remanent magnetisation, *Earth Planet. Sci. Lett.*, *189*, 269–276, 2001.
- Moskowitz, B., R. B. Frankel, D. A. Bazylinski, H. W. Jannasch, and D. R. Lovley, A comparison of magnetite particles produced anaerobically by magnetotactic and dissimilatory iron-reducing bacteria, *Geophys. Res. Lett.*, *16*, 665–668, 1989.
- Moskowitz, B. M., Rock magnetic criteria for the detection of biogenic magnetite, *Earth Planet. Sci. Lett.*, *120*, 283–300, 1993.
- Passier, H. F., Sulphur geochemistry and sapropel formation, syngenetic and diagenetic signals in eastern Mediterranean sediments, Ph.D. thesis, Utrecht University, Utrecht, Netherlands, 1998.
- Passier, H. F., G. J. de Lange, M. J. Dekkers Magnetic properties and geochemistry of the active oxidation front and the youngest sapropel in the eastern Mediterranean Sea, *Geophys. J. Int.*, *145*, 604–614, 2001.
- Pike, C. R., A. P. Roberts, and K. L. Verosub, Characterizing interactions in fine magnetic particle systems using first order reversal curves, *J. Appl. Phys.*, *85*, 6660–6667, 1999.
- Roberts, A. P., C. R. Pike, and K. L. Verosub, First-order reversal curve diagrams: A new tool for characterizing the magnetic properties of natural samples, *J. Geophys. Res.*, *102*, 28,461–28,475, 2000.
- Robertson, D. J., and D. E. France, Discrimination of remanence-carrying minerals in mixtures, using isothermal remanent magnetisation acquisition curves, *Phys. Earth Planet. Inter.*, *82*, 223–234, 1994.
- Rohling, E. J., Review and new aspects concerning the formation of eastern Mediterranean sapropels, *Mar. Geol.*, *122*, 1–28, 1994.
- Rosignol-Strick, M., W. Nesteroff, P. Olive, and C. Vergnaud-Grazzini, After the deluge: Mediterranean stagnation and sapropel formation, *Nature*, *295*, 105–110, 1982.
- Schmidt, A. M., T. Von Dobeneck, and U. Bleil, Magnetic characterization of Holocene sedimentation in the South Atlantic, *Paleoceanography*, *14*, 465–481, 1999.
- Schwartz, M., S. P. Lund, D. E. Hammond, R. Schwartz, and K. Wong, Early sediment diagenesis on the Blake/Bahama Outer Ridge, North Atlantic Ocean, and its effects on sediment magnetism, *J. Geophys. Res.*, *102*, 7903–7914, 1997.
- Tarduno, J. A., and S. L. Wilkison, Non-steady state magnetic mineral reduction, chemical lock-in, and delayed remanence acquisition in pelagic sediments, *Earth Planet. Sci. Lett.*, *144*, 315–326, 1996.
- Tarduno, J. A., W. Tian, and S. Wilkison, Biogeochemical remanent magnetization in pelagic sediments of the western equatorial Pacific Ocean, *Geophys. Res. Lett.*, *25*, 3987–3990, 1998.
- Tauxe, L., T. A. T. Mullender, and T. Pick, Potbellies, wasp-waists, and superparamagnetism in magnetic hysteresis, *J. Geophys. Res.*, *101*, 571–583, 1996.
- Thompson, R., and F. Oldfield, *Environmental Magnetism*, 227 pp., Allen and Unwin, Concord, Mass., 1986.
- Walden, J., and K. White, Investigation of the controls on dune colour in the Namib Sand Sea using mineral magnetic analyses, *Earth Planet. Sci. Lett.*, *152*, 187–201, 1997.